

The unreasonable effectiveness of the $n\Sigma v$ approximation

ELISHA MODELEVSKY ¹, NICHOLAS C. STONE ^{2,1} AND RE'EM SARI ¹

¹*Racah Institute of Physics, The Hebrew University, 91904, Jerusalem, Israel*

²*Department of Astronomy, University of Wisconsin, Madison, WI, 53706*

Submitted to ApJ

ABSTRACT

In kinetic theory, the classic $n\Sigma v$ approach calculates the rate of particle interactions from local quantities: the number density of particles n , the cross-section Σ , and the average relative speed v . In stellar dynamics, this formula is often applied to problems in collisional (i.e. dense) environments such as globular and nuclear star clusters, where blue stragglers, tidal capture binaries, binary ionizations, and micro-tidal disruptions arise from rare close encounters. The local $n\Sigma v$ approach implicitly assumes the ergodic hypothesis, which is not well motivated for the densest star systems in the Universe. In the centers of globular and nuclear star clusters, orbits close into 1D ellipses because of the degeneracy of the potential (either Keplerian or harmonic). We find that the interaction rate in perfectly Keplerian or harmonic potentials is determined by a global quantity – the number of orbital intersections – and that this rate can be far lower or higher than the ergodic $n\Sigma v$ estimate. However, we find that in most astrophysical systems, deviations from a perfectly Keplerian or harmonic potential (due to e.g. granularity or extended mass) trigger sufficient orbital precession to recover the $n\Sigma v$ interaction rate. Astrophysically relevant failures of the $n\Sigma v$ approach only seem to occur for tightly bound stars orbiting intermediate-mass black holes, or for the high-mass end of collisional cascades in certain debris disks.

Keywords: Stellar kinematics (1608) — Celestial mechanics (211)

1. INTRODUCTION

Dense star systems are often termed “collisional” because of the dominant role that pairwise gravitational scatterings play in determining their bulk evolution. However, these star clusters are also collisional in a second sense: their high density leads to a significant rate of close encounters between stellar-mass objects, including (but not limited to) physical collisions. These close encounters can shape the properties of cluster members: in globular clusters, non-destructive star-star collisions produce easily identifiable blue stragglers (Hills & Day 1976; Baily 1995), while in the dynamically “hotter” environments of galactic nuclei, physical collisions between pairs of stars may produce luminous transients (Balberg et al. 2013; Balberg & Yassar 2023; Brutman

et al. 2024) or destroy red giant envelopes (Dale et al. 2009). Likewise, close star-binary interactions ionize wide binaries, harden tight binaries, and preferentially swap light stars out of pre-existing binary systems (Heggie 1975; Goodman & Hut 1989; Ivanova et al. 2005).

Close encounters between combinations of stars and stellar mass compact objects may also lead to the production of interesting high energy astrophysical sources. Observations have long established that cataclysmic variables and neutron star X-ray binaries are massively over-represented in the dense cores of globular clusters (Clark 1975; Grindlay et al. 2001; Pooley et al. 2003), while a similar over-representation has more recently been identified for black hole X-ray binaries in the Milky Way’s nuclear star cluster (Hailey et al. 2018). The origins of these overabundances are likely dynamical and linked to frequent close encounters, although past models have debated the relative importance of two-body tidal captures (Fabian et al. 1975; Press & Teukolsky

1977; Generozov et al. 2018) and three-body binary-single scatterings (Hills 1976; Ivanova et al. 2006, 2008; Kremer et al. 2020). The discoveries of gravitational wave emission from binary black hole mergers have also drawn much attention to dynamical formation of binary black holes via repeated binary-single scatterings in globular (Portegies Zwart & McMillan 2000; Rodriguez et al. 2016) and nuclear (Antonini & Rasio 2016) star clusters.

All of these interesting astrophysical phenomena are driven by close encounters of particles in dense environments, and their rates have all been calculated in past works using the standard “ $n\Sigma v$ ” kinetic approach. Specifically, in a gas with particle number density n , the rate of collisions per particle is $n\Sigma v$, where Σ is the collision cross-section and v is the mean relative speed of particles in the gas. This statistical approach is widely used in gas and plasma kinetic theory, but also appears naturally well-suited for estimating encounter rates in stellar kinetic theory, and appears to be in good agreement with direct N-body simulations in those contexts for which it has been tested (Reinoso et al. 2022).

However, a crucial assumption behind the $n\Sigma v$ formalism is the uniformity of particles in space. In essence, this is the ergodic hypothesis – all microstates are equiprobable over long periods of time; or in another formulation, long time averages are equivalent to averages over the statistical ensemble. While the ergodic hypothesis is suitable for a chaotic gas (Boltzmann’s “Stosszahlansatz”), it will not be correct for every multi-particle system. In systems where particles move in a degenerate potential, particle trajectories may be confined to restricted regions in phase space, and some regions in space will never be occupied (for a given realization of the system).

In this article we will focus on three types of astrophysical potentials, with increasing levels of degeneracy:

1. Spherically symmetric potentials: trajectories are confined to a single plane of motion.
2. Kepler potential: trajectories are closed planar orbits.
3. Harmonic potential: trajectories are closed planar orbits, and *all* trajectories have the same period.

The Kepler potential ($\Phi \propto r^{-1}$) and the harmonic potential ($\Phi \propto r^2$) are the only two spherically symmetric potentials that exhibit closed orbits (Bertrand 1873; Chin 2015), so this is a complete set of degenerate potentials.

Although they may appear fine-tuned, these potentials are accurate (sometimes highly accurate) approxi-

mations for many multi-particle systems in astrophysics. Planetary orbits in the solar system are governed by the Sun’s Kepler potential, just as stellar trajectories in the vicinity of a supermassive black hole are governed by its Kepler potential. Near the centers of globular clusters and nuclear star clusters (at least, those lacking a central massive black hole), stars will relax into a constant-density core, creating a harmonic gravitational potential (Spitzer & Hart 1971). Further away from the center of such clusters, the gravitational potential is not harmonic, but is still spherically symmetric. Rather than representing some sort of unusual edge case, *these degenerate potentials describe the densest star systems in the Universe*, highlighting their importance for a full understanding of astrophysical close encounter rates.

In section 2, we study how the collision rate in such degenerate systems differs from ergodic systems. In section 3 we examine how precession (which removes the degeneracy) affects the collision rate. Finally, in section 4, we apply these results to realistic astrophysical systems.

2. COLLISION RATE IN DEGENERATE SYSTEMS

2.1. Spherically symmetric potentials

Trajectories in a spherically symmetric potential are confined to a single plane of motion, as radial forces cannot torque an orbital angular momentum vector. In this subsection, we examine how collisions behave under these conditions.

Here we assume that each particle’s trajectory is ergodic inside its fixed plane of motion. In other words, we will use an in-plane areal density function $g(r)$ to describe the probability of finding a particle in an thin annulus of radius r . $g(r)$ is related to the volumetric density distribution $n(r)$, describing the ensemble-averaged density of finding a particle in a thin shell of radius r . More quantitatively, said probability is $g(r)2\pi r dr = n(r)4\pi r^2 dr$, so that $g(r) = 2rn(r)$.

Now let us consider two particles, each with its own plane of motion. Denoting the angle between the planes by α , it is evident that the smaller α is, the higher the collision rate between the particles will be. For $\alpha = 0$, the co-planar case, we can perform a planar $n\Sigma v$ calculation to evaluate the collision rate, with the planar cross-section $\Sigma_{2d} = 2D$.

$$\begin{aligned} \text{co-planar rate} &= \int d^2\vec{r} g_1 g_2 \Sigma_{2d} v = \Sigma_{2d} \int 2\pi r (2rn(r))^2 v(r) dr \\ &= 16\pi D \int n^2 r^3 v dr. \end{aligned} \tag{1}$$

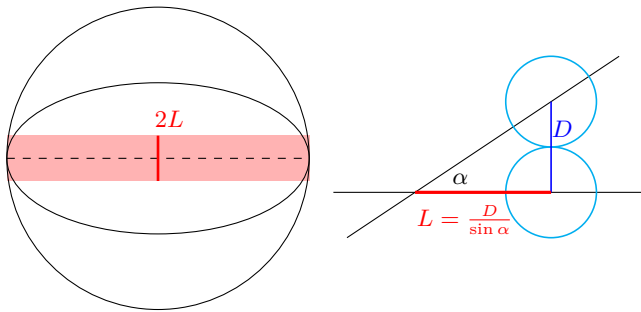


Figure 1. On the left – two planes intersecting (represented by the black ellipses). The red area is where collisions can happen. On the right – a view from the side of the intersecting planes (the black lines). L is the largest distance from the intersection where two particles with diameter D can collide.

Compare this to the mean ergodic rate, calculated using a volumetric $n\Sigma v$, with $\Sigma_{3d} = \pi D^2$.

$$\begin{aligned} \text{mean rate} &= \int d^3\vec{r} n_1 n_2 \Sigma_{3d} v = \Sigma_{3d} \int 4\pi r^2 n^2 v dr \\ &= 4\pi^2 D^2 \int n^2 r^2 v dr. \end{aligned} \quad (2)$$

Their ratio is

$$\frac{\text{co-planar rate}}{\text{mean rate}} = \frac{4}{\pi D} \frac{\int n^2 r^3 v dr}{\int n^2 r^2 v dr} \sim \frac{R}{D}, \quad (3)$$

where R is the characteristic radius of the particles' trajectories.

For a general angle α , two planes intersect on a single line. The greatest distance from this line where intersections can happen is $L = \frac{D}{\sin \alpha}$ (see figure 1). The rate of collisions, compared to the rate where $\alpha = 0$, is the ratio between the area where collisions can happen, to the total area where a particle can be. When $L/R > 1$, this ratio is close to unity; otherwise, this ratio is $\sim L/R$. Therefore, the rate of collisions for particles at planes with relative angle α is:

$$\text{rate}(\alpha) \sim n\Sigma v \begin{cases} \frac{R}{D} & \text{if } \sin \alpha < \frac{D}{R} \\ \frac{1}{\sin \alpha} & \text{if } \sin \alpha > \frac{D}{R} \end{cases} \quad (4)$$

For particles with planes close to being parallel, the collision rate is greater than the ergodic rate by a factor of $\sim R/D$, but they are scarce. The probability of the relative angle between planes to be $\alpha < \frac{D}{R}$ is $\sim \frac{D^2}{2R^2}$. Thus, the contribution of such collisions is $\sim \frac{D}{R} \ll 1$ of the total rate.

2.2. Kepler potential: closed orbits

The Kepler potential is more degenerate than a general spherically symmetric potential, resulting in closed

orbits. This time we will use an even weaker ergodic hypothesis – ergodicity along the closed orbit¹. That is, we will assume that particles' appearances along their trajectory can be described by a time-independent probability distribution. This probability function is $f = 1/vT$, where v is the speed at a point along the orbit, and T is the orbital period.

Analogously to subsection 2.1, let us first estimate the collision rate between two particles that share the same orbit.

$$\text{co-orbital rate} = \oint dl f_1 f_2 \Sigma_{1d} w \sim \frac{2\pi R w}{(vT)^2} \sim \frac{w}{v} T^{-1}, \quad (5)$$

where $\Sigma_{1d} = 1$ is the linear “cross-section” (note that for perfectly closed orbits, this is just a binary δ -function), $w = |\vec{v}_1 - \vec{v}_2|$ is the relative speed, and $2\pi R$ is the approximate length of the orbit. That is, if the two particles are not moving in the same direction along the orbit, they will collide twice every period.

In the general case of two particles in different orbits, a collision is only possible if the two orbits intersect. For our purposes, we define an intersection to be a local minimum of the distance between the two orbits Δ , where $\Delta < D$.

The portion of a trajectory where a collision can occur is of length $2\sqrt{D^2 - \Delta^2} \csc \alpha$, where α is the angle between the trajectories at their closest point. Thus, the collision rate due to an intersection of distinct closed orbits is

$$\begin{aligned} \text{collision rate of intersection} &= \int dl \frac{\Sigma_{1d} w}{v_1 T_1 v_2 T_2} \\ &= \frac{2w\sqrt{D^2 - \Delta^2}}{v_1 T_1 v_2 T_2 \sin \alpha}. \end{aligned} \quad (6)$$

It should be noted that for very small angles α , this formula can predict a rate much greater than either of T_i^{-1} . In such cases, equation 6 would not be applicable since the formula for the length of the intersection region is only valid when this region is small in comparison to the entire orbit.

A rough approximation of equation 6 gives

$$\text{collision rate of intersection} \sim \frac{D}{vT^2} \sim \frac{D}{R} T^{-1}. \quad (7)$$

The expected number of intersections $\langle N_{int} \rangle$ in a system with N particles is roughly $\sim N^2 \frac{D}{R}$, giving an av-

¹ Note that this hypothesis will not be valid for two closed orbits with a rational period commensurability, i.e. a mean motion resonance.

verage total collision rate of

$$\begin{aligned} \text{mean total rate} &= \langle N_{int} \rangle \cdot \text{collision rate of intersection} \\ &\sim \frac{N^2 D^2}{R^2 T} \sim N n \Sigma v. \end{aligned} \quad (8)$$

See appendix A for a general proof that $n \Sigma v$ is always correct in an ensemble average. Note that the expected number of intersections may be < 1 in some systems. Most realisations of such systems will not have collisions at all; conversely, some realisations will have a rate of collisions far greater than $N n \Sigma v$, with intersections yielding collisions repeatedly.

2.3. Harmonic potential: closed orbits, universal period

The harmonic potential, besides having closed orbits, has another important feature that distinguishes its behavior from the Kepler potential. Because all trajectories have the same period, the assumption of ergodicity inside the orbit is no longer valid. That is because even if two orbits intersect, they will either collide every period or never collide.

Given an intersection of orbits, the probability of the relative orbital phase allowing collisions is $\sim D/R$. The expected number of such *opportunities* (intersection plus phase coincidence) is $\frac{D}{R} \langle N_{int} \rangle \sim N^2 \left(\frac{D}{R}\right)^2$.

2.4. Summary of degenerate potential dynamics

Each of the degenerate potentials discussed in this section has a special case where pairwise collision rates are enhanced. In general spherically symmetric potentials, this is when the two particles are coplanar. In the Kepler potential, this is when the orbits intersect. In the harmonic potential, this case is when the orbits intersect and their relative phase permits collisions.

Table 1 summarizes the probability and collision rates of each case. Multiplying the probabilities by the pairwise collision rate, we can see that regardless of the potential, the expected collision rate of a pair is $\sim \left(\frac{D}{R}\right)^2 T^{-1}$.

The essential difference between the Kepler or harmonic potentials, and the general or spherical potentials, is the type of pair that contributes most of the collisions. In a general or a spherical potential, most collisions come from generic orbital pairings; conversely, in the Kepler or harmonic potentials, collisions come from rare types of orbit pairs, colliding repeatedly. This is why in a general or in a spherical potential, different realizations will have roughly the same collision rate; while in the Kepler or in the harmonic potential, different realizations may have very different collision rates.

3. THE ROLE OF DESTRUCTIVE COLLISIONS AND ORBITAL PRECESSION

Up to now, we have discussed dynamical systems with perfect potentials and non-destructive (repeatable) collisions. In this section, we will consider two more realistic effects – destructive collisions and orbital precession.

In closed-orbit systems (Kepler and harmonic, see subsection 2.4), collisions happen between the same particles (those with intersecting orbits) over and over again. In light of this, the rate of collisions in such systems should be drastically diminished if collisions are *destructive*.

For the following discussion, to unify the treatment of the Kepler and the harmonic potential, let us call the situation where a pair of particles can collide an *opportunity*. An opportunity is an intersection for the Kepler potential, and an intersection with aligned phase for the harmonic potential.

Once the system is formed, it is only a matter of time until all opportunities yield a collision, and there will be no more collisions. We call the characteristic time for an opportunity to yield a collision the *depletion time*, t_{dep} . The depletion time is the inverse of the collision rate for an opportunity.

$$t_{dep} = \begin{cases} \frac{R}{D} T & \text{Kepler} \\ T & \text{harmonic} \end{cases} \quad (9)$$

As a rough approximation, for a duration of t_{dep} since the creation of the system, the rate of collisions is $\sim \frac{N_{op}}{t_{dep}}$ (where N_{op} is the number of opportunities), and after that there are no collisions anymore. Let us recall that the expected value of N_{op} is

$$\langle N_{op} \rangle = \begin{cases} N^2 \frac{D}{R} & \text{Kepler} \\ N^2 \left(\frac{D}{R}\right)^2 & \text{harmonic} \end{cases} \quad (10)$$

Now let us consider systems that are only approximately Keplerian or harmonic, where orbits precess with a precession time of $t_{prec} \gg T$. For now, let us assume that precession alters the orbit, without changing the phase.

Precession effectively “refreshes” the orbits, in the sense that old opportunities may disappear as new opportunities arise. The characteristic time for opportunities to change due to precession will be called the *refresh time*, and we shall denote it by t_{ref} . Note that t_{ref} is smaller than the usual precession time t_{prec} , which signifies the time required for major changes in orbit to take place: $t_{ref} \sim \frac{D}{R} t_{prec}$. This is because a displacement of order D is enough to remove existing intersections and create new ones.

Pair type	Probability	Collision rate			
		General potential	Spherical	Kepler	Harmonic
common	1	$(\frac{D}{R})^2 T^{-1}$	$(\frac{D}{R})^2 T^{-1}$	0	0
co-planar	$(\frac{D}{R})^2$		$\frac{D}{R} T^{-1}$	0	0
intersecting	$\frac{D}{R}$			$\frac{D}{R} T^{-1}$	0
intersecting + phase	$(\frac{D}{R})^2$				T^{-1}

Table 1. Types of particle pairs, their probability and their per-particle collision rate in different potentials. A common pair is the most likely case, a co-planar pair is when both particles are in the same plane (up to an angle of D/R), an intersecting pair is when the orbits intersect, and an intersecting + phase aligned pair is when the orbits intersect and the particles pass at the intersection at the same time. For each potential, the green cell is the type of pair that contributes the most to collision rate. We note that this table focuses on idealized potentials, neglecting complications due to destructive collisions, orbital precession, etc.

Once there are opportunities, they yield collisions until they are depleted after a time t_{dep} ; after a time t_{ref} , new opportunities are formed. If $t_{\text{ref}} > t_{\text{dep}}$, the true (“refresh-limited”) collision rate will be

$$\text{total collision rate} = \frac{\langle N_{\text{op}} \rangle}{t_{\text{ref}}} = N^2 \frac{D}{R} t_{\text{ref}}^{-1} \begin{cases} 1 & \text{Kepler} \\ \frac{D}{R} & \text{Harmonic} \end{cases}. \quad (11)$$

This can be compared to the $n\Sigma v$ calculation by using $\Sigma \sim D^2$, $n \sim N/R^3$ and $v \sim R/T$.

$$\begin{aligned} \text{total collision rate} &= Nn\Sigma v \frac{t_{\text{dep}}}{t_{\text{ref}}} \\ &= Nn\Sigma v \frac{T}{t_{\text{ref}}} \begin{cases} \frac{R}{D} & \text{Kepler} \\ 1 & \text{Harmonic} \end{cases}. \end{aligned} \quad (12)$$

3.1. Other causes for orbit shuffling

Precession coherently changes the orientation of orbits. Therefore, the time required for a change of order $\delta \ll 1$ in the orbital parameters is $\delta \cdot t_{\text{prec}}$; this is why $t_{\text{ref}} = \frac{D}{R} t_{\text{prec}}$.

On the other hand, other causes of orbital changes are random in nature, and behave like a random walk or a diffusion process. The most relevant example is weak scatterings from individual particles in a many-body gravitational system. The time for such scatterings to make an order unity change to orbital parameters is the relaxation time, t_{relax} . The required time for a change of order δ in this case is $\delta^2 \cdot t_{\text{relax}}$. Hence,

$$t_{\text{ref}} = \left(\frac{D}{R}\right)^2 t_{\text{relax}}. \quad (13)$$

It should be noted that equation 13 is only valid in the diffusion limit, i.e. when a single random walk “step” is small compared to δ . When this is not the case, t_{ref} must be calculated according to the specifics of the random walk process, and in particular the way a random walk step affects the trajectory. The simplest situation

is where each step occurs instantaneously (compared to the trajectory time scale T); then t_{ref} will be the average time between steps.

3.2. Imperfect harmonic systems

In the centers of realistic star clusters, the potential will be close to a harmonic potential, but not perfectly harmonic. In such cases, the imperfection of the potential will cause two effects – precession, and deviations from the universal frequency. We have already discussed the role of precession; in this subsection, we will discuss the effect that deviations from the universal frequency have on the collision rate in nearly harmonic systems.

Let us denote the characteristic deviation from the universal frequency by ε , i.e. given two particles, their period ratio will be $\sim 1 + \varepsilon$. If $\varepsilon \gtrsim \frac{D}{R}$, the system is effectively not harmonic, since after one “universal” period a particle will no longer overlap its previous position at all. Such a system will no longer exhibit “harmonic” behaviour (closed orbits plus a universal frequency), and will behave more like a “Keplerian” system (possessing just closed orbits): an opportunity will be any intersection, and the depletion time will be $T \frac{R}{D}$.

On the other hand, if $\varepsilon \ll \frac{D}{R}$, there are several different cases, depending on the value of $\varepsilon \frac{t_{\text{ref}}}{T}$ – the change in phase during a refresh time. If $\varepsilon \frac{t_{\text{ref}}}{T} < \frac{D}{R}$, phase changes are minor in a refresh time. In this case, variations in orbital periods are negligible and the system can be considered harmonic.

If $\frac{D}{R} < \varepsilon \frac{t_{\text{ref}}}{T} < 1$, not every intersection will be an opportunity, but the phase match for an opportunity is more lenient than $\frac{D}{R}$. In this case, the expected number of opportunities is $\langle N_{\text{op}} \rangle = N^2 \frac{D}{R} \varepsilon \frac{t_{\text{ref}}}{T} > \langle N_{\text{op}} \rangle_{\text{Harmonic}}$, and the collision rate is

$$\text{total collision rate} = \frac{\langle N_{\text{op}} \rangle}{t_{\text{ref}}} = \varepsilon N^2 \frac{D}{R} T^{-1}. \quad (14)$$

We call this type of behavior *semi-harmonic*.

	Globular	Nuclear
Core radius r_c	1 pc	2-5 pc
Total mass M	$10^5 M_\odot$	$10^6 - 10^8 M_\odot$
Central density ρ_c	$5 \cdot 10^3 M_\odot \text{pc}^{-3}$	$10^3 - 10^5 M_\odot \text{pc}^{-3}$

Table 2. Properties of globular clusters and nuclear star clusters. The values for globular clusters are from Binney & Tremaine (2008) and the values for NSCs are from Neumayer et al. (2020).

Finally, if $\varepsilon \frac{t_{\text{ref}}}{T} > 1$, then any intersection will yield a collision in a refresh time – so every intersection is an opportunity, like in a Kepler potential.

Figure 2 schematically summarizes the conditions for each type of behaviour.

4. ASTROPHYSICAL EXAMPLES

In this section, we will explore some examples of multi-particle astrophysical systems that are governed by a Kepler or a harmonic potential (to leading order).

4.1. Nearly isothermal star clusters

In self-gravitating systems, a spherically symmetric, uniform density distribution creates a harmonic potential. While star clusters are not uniform density systems in general, the process of collisional relaxation will, over time, transform arbitrary initial distributions of stars into an isothermal distribution, with a constant density core surrounded by a non-uniform halo (Spitzer & Hart 1971). Because relaxation times scale inversely with stellar densities, it is the densest star systems – ones where $n\Sigma v$ close encounter rates are high – that will be most able to achieve isothermal, constant density cores over a Hubble time. Globular clusters and nuclear star clusters (NSCs) are the densest star systems in the Universe, are often approximately spherical, and possess cores with approximately uniform density; we will parametrize core properties with a core radius r_c , and a central mass density ρ_c . Characteristic values are shown in table 2.

As the central potential inside an astrophysical cluster is only approximately harmonic, we will use the method outlined in figure 2 to determine the collision rate. First, we must identify sources of orbit shuffling and estimate t_{ref} . The two main sources would be *mass precession* due to the true density profile deviating from a uniform distribution, and the effect of *granularity* – gravitational encounters with individual stars in the cluster.

The refresh time due to the granularity of the gravitational potential can be derived from the relaxation time of a weakly collisional system (Binney & Tremaine

2008)

$$t_{\text{relax}} = \frac{0.1N(r)}{\log N(r)} T \approx \frac{0.1N}{\log N} \left(\frac{r}{r_c} \right)^3 T, \quad (15)$$

where $N(r)$ is the number of stars up to a distance of r from the center, and N is the total number of stars. As discussed in subsection 3.1, this gives a refresh time of

$$\begin{aligned} t_{\text{ref}}^{\text{gran}} &= \left(\frac{D}{r} \right)^2 t_{\text{relax}} = \frac{0.1N}{\log N} \frac{r}{r_c} \left(\frac{D}{r_c} \right)^2 T \\ &= 2 \cdot 10^{-16} \frac{N}{\log N} \frac{r}{r_c} \left(\frac{D}{2R_\odot} \right)^2 \left(\frac{r_c}{1 \text{ pc}} \right)^{-2} T. \end{aligned} \quad (16)$$

The relaxational refresh time is thus very short in realistic constant density cores. Stars, even red supergiants with $D = 3 \cdot 10^3 R_\odot$ (Levesque et al. 2005), will always be too small for the refresh time to be longer than a period (see table 2 for values of N and r_c).

If instead of considering stellar collisions, we look for disruptions (or “ionizations”) of binary pairs, the cross-section becomes much greater since D will be half the separation between the stars. An upper bound for the separation of a long-lived binary star system is given by the “hard-soft boundary” (Heggie 1975; Fregeau et al. 2006): $Gm_B/a_B > \sigma^2$, where m_B is the binary’s mass, a_B is its’ semi-major axis, and $\sigma^2 \sim GM_c/r_c$ is the velocity dispersion in the cluster core. Thus, for binary disruptions,

$$D \sim a_B < \frac{m_B}{M_c} r_c = \frac{m_B}{N\bar{m}} r_c, \quad (17)$$

where \bar{m} is the mean mass of stars in the cluster. Plugging this into equation 16,

$$\frac{t_{\text{ref}}}{T} = \frac{0.1}{N \log N} \frac{r}{r_c} \left(\frac{m_B}{\bar{m}} \right)^2. \quad (18)$$

The largest plausible $\frac{m_B}{\bar{m}}$ is $\sim 10^2$ (for a binary containing a large stellar mass black hole), so for any value of N in the range ($10^5, 10^8$), the refresh time is still shorter than the period.

In conclusion, $n\Sigma v$ collision rate calculations are always highly valid in star clusters, due to the effect of granularity².

4.2. Supermassive Black Holes

In the nearly Keplerian potential of an SMBH, orbits come close to closing, but different forms of precession play an important role in regulating collision rates, as we show here.

² We have not taken into account mass precession which is another major source of orbit shuffling, since granularity is strong enough by itself. Mass precession would restore the $n\Sigma v$ limit by itself, except for orbits very close to the center.

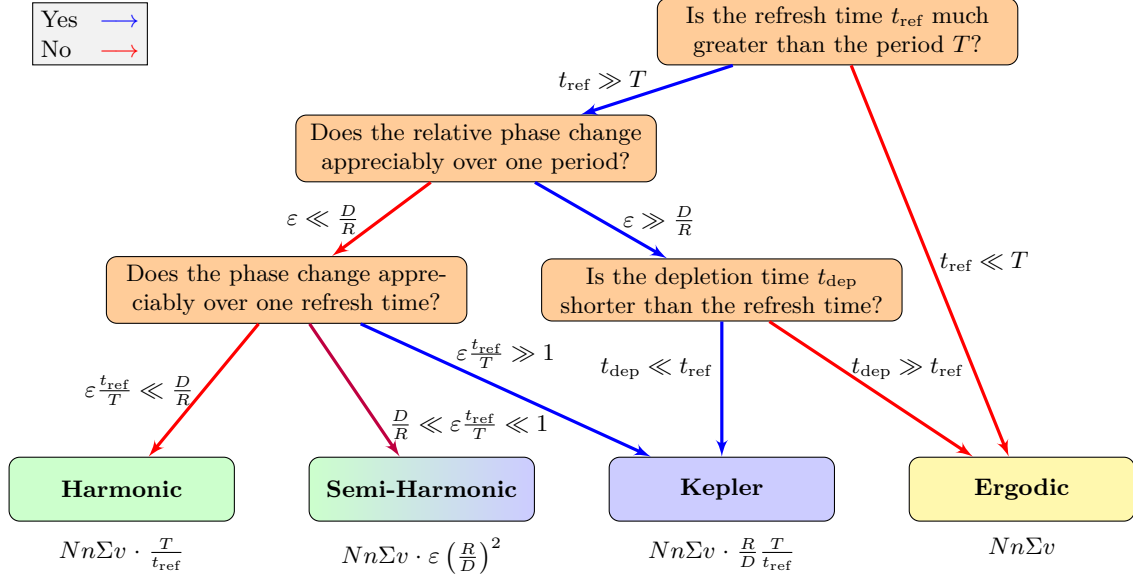


Figure 2. A flow chart summarizing the collision dynamics that different systems will exhibit, and the total collision rate for each type of dense star cluster.

4.2.1. Stellar collisions around a SMBH

For stars orbiting a SMBH, the dominant effects that cause precession are the collective gravitational potential of all other nearby stars, and general relativistic corrections to the SMBH’s nearly Keplerian potential (Merritt et al. 2010). The precession due to other stars’ gravity, which is often called *mass precession*, sets an upper bound for the radius r where non-ergodic behavior may occur; conversely, precession from general relativity (GR) sets a lower bound on these radii. We show in appendix B that, while stellar granularity/relaxation can sometimes play a role in refreshing orbital intersections, it is always subdominant to mass precession in situations of interest (unlike the situation in isothermal star clusters).

Let us assume a power-law density distribution $n \sim r^{-\alpha}$ for stars around the SMBH (in a relaxed single-species stationary state, $\alpha = 7/4$; Bahcall & Wolf 1976), normalized using a quasi-empirical formula for the influence radius $R_{\text{inf}} = 1 \text{ pc} \sqrt{\frac{M_{\bullet}}{10^6 M_{\odot}}}$ (Stone & Metzger 2016). The influence radius is defined as the radius inside of which the enclosed stellar mass $M(r)$ equals the SMBH mass M_{\bullet} . Assuming that the mean stellar mass does not depend on the distance from the SMBH, this gives an enclosed-mass profile

$$M(r) = M_{\bullet} \left(\frac{r}{R_{\text{inf}}} \right)^{3-\alpha} = M_{\bullet} \left(\frac{M_{\bullet}}{10^6 M_{\odot}} \right)^{\frac{\alpha-3}{2}} \left(\frac{r}{1 \text{ pc}} \right)^{3-\alpha}. \quad (19)$$

The mass precession time inside the radius of influence is $t_{\text{prec}}^{\text{mass}} \sim \frac{M_{\bullet}}{M(r)} T$, which leads to a refresh time of

$$t_{\text{ref}}^{\text{mass}} \sim \frac{D}{r} \frac{M_{\bullet}}{M(r)} T, \quad (20)$$

and a depletion/refresh time ratio of

$$\begin{aligned} \frac{t_{\text{dep}}}{t_{\text{ref}}^{\text{mass}}} &= \left(\frac{r}{D} \right)^2 \frac{M(r)}{M_{\bullet}} \\ &= 5 \cdot 10^{14} \left(\frac{D}{2R_{\odot}} \right)^{-2} \left(\frac{M_{\bullet}}{10^6 M_{\odot}} \right)^{\frac{\alpha-3}{2}} \left(\frac{r}{1 \text{ pc}} \right)^{5-\alpha}. \end{aligned} \quad (21)$$

In contrast, the GR precession time is $\sim \frac{r}{R_{\text{BH}}} T$, where $R_{\text{BH}} = \frac{2GM_{\bullet}}{c^2}$ is the Schwarzschild radius of the black hole. So, the refresh time is

$$t_{\text{ref}}^{\text{GR}} \sim 0.5 \left(\frac{D}{2R_{\odot}} \right) \left(\frac{M_{\bullet}}{10^6 M_{\odot}} \right)^{-1} T. \quad (22)$$

The depletion/refresh time ratio is thus

$$\frac{t_{\text{dep}}}{t_{\text{ref}}^{\text{GR}}} = 2 \left(\frac{D}{2R_{\odot}} \right)^{-1} \frac{r}{D} \left(\frac{M_{\bullet}}{10^6 M_{\odot}} \right). \quad (23)$$

From equation 23, it is evident that, for Sun-like stars around SMBHs, the depletion time will always be much greater than the GR refresh time. Red supergiants on the other hand, can have a diameter up to 3 orders of magnitude greater than R_{\odot} . Figure 3 shows the ratio between depletion time and refresh time for different values of D , as functions of SMBH mass and distance from it. Relevant radii must be greater than the

Schwarzschild radius $\frac{2GM_\bullet}{c^2}$ and the tidal disruption radius $\frac{D}{2} \left(\frac{M_\bullet}{M_\star}\right)^{\frac{1}{3}}$, otherwise the stars will not survive long enough for collisions to be important.

The results shown in figure 3 also take into account gravitational focusing, which increases the effective collisional diameter of the star according to

$$D_{eff} = D \cdot \sqrt{1 + \left(\frac{v_{esc}}{v_{rel}}\right)^2} \approx D \sqrt{1 + 10^2 \frac{\left(\frac{M_\star}{M_\odot}\right) \left(\frac{r}{1 \text{ pc}}\right)}{\left(\frac{M_\bullet}{10^6 M_\odot}\right) \left(\frac{D}{2R_\star}\right)}, \quad (24)$$

where $v_{esc} = \sqrt{4GM_\star/D}$ is the escape velocity from the surface of the star, and $v_{rel} \approx \sqrt{GM_\bullet/r}$ is the relative velocity of colliding stars.

Under these constraints, there are small regions of parameter space where $t_{dep} < t_{ref}$. In general, such regions will exist for *intermediate mass black holes* with masses $M_\bullet < 10^6 M_\odot$, and radii not much larger than the tidal disruption radius. An extreme example in figure 3 is of $M_\bullet = 10^4 M_\odot$, $D = 200R_\odot$, and $r = 5 \cdot 10^{-5} \text{ pc} = 10 \text{ AU}$, where the ratio t_{ref}/t_{dep} is as large as $\sim 10^2$. By equation 12, this amounts to a reduction of collision rates by a factor of 10^{-2} in this region.

Note that a common assumption in each panel of figure 3 is that the star's mass $M_\star = 1M_\odot$; the star's mass M_\star is only relevant for the tidal disruption radius, so for more massive stars, there is a bigger part of parameter space where $t_{dep} < t_{ref}$. Likewise, we assume orbits have a single characteristic radius for simplicity.

4.2.2. Binary disruptions around a SMBH

The interaction cross-section for collisional ionization of a binary can be much greater than that for direct physical collisions with a star. In this case, D would be, roughly, the separation between the stars in the binary system. The possibility of the SMBH tidally disrupting the binary sets an upper bound for the possible separation in a given radius

$$D_{max} = r \left(\frac{m_B}{M_\bullet}\right)^{\frac{1}{3}}, \quad (25)$$

where m_B is the mass of the binary.

Figure 4 shows the ratio between refresh time and depletion time for binaries with the maximal separation (by equation 25). It can be seen that for black hole masses of less than $10^6 M_\odot$, there is a spatial region where refresh times can be greater than the depletion time, and non-ergodic collisional behavior may occur.

Intermediate mass black holes with $M_\bullet \lesssim 10^5 M_\odot$ exhibit a significant range of radii where binaries will experience collisional ionization at rates 1-2 orders of magnitude below the $n\Sigma v$ prediction. For significantly more massive SMBHs, the ergodic calculation of collision rates will always be appropriate.

4.3. Planetesimals around a massive star

Planetesimals in asteroid belts or in debris disks around a star move in a nearly Keplerian potential. Over long timescales, the size distribution of these planetesimals will evolve in a collisional cascade, eventually reaching a steady state in mass flux due to collisional fragmentation (Dohnanyi 1969). The detailed shape of this steady state particle size distribution is a function of the collision rate, which is generally computed in the $n\Sigma v$ way (Tanaka et al. 1996; Pan & Sari 2005; Schlichting et al. 2013). It is therefore interesting to understand when the standard approach can be applied.

In the asteroid belt of a planetary system, the main sources of precession are GR and perturbations from a massive planet, if one exists. In a tightly bound debris disk around a star, the main sources of precession are GR, the disk's gravitation, and the star's quadrupole moment. In this section, we explore the conditions under which the $n\Sigma v$ treatment of collision rates can be applied to collisional cascades in various debris disks.

4.3.1. Asteroid belt in a planetary system

Taking equation 23 for GR precession, and modifying its normalizations to be more suitable for the case of an asteroid belt in a planetary system, we get

$$\frac{t_{dep}}{t_{ref}^{GR}} = 4 \cdot 10^8 \left(\frac{D}{1 \text{ km}}\right)^{-2} \left(\frac{r}{1 \text{ AU}}\right) \left(\frac{M_\star}{M_\odot}\right), \quad (26)$$

where M_\star is the mass of the central star. If the central star has mass similar to our sun, and the orbit radius is of about 1 AU, this ratio would be less than 1 only for planetesimals with a diameter D of at least 10^4 km , comparable to the Earth.

An important mechanism that could lengthen the refresh time is low orbital eccentricity e , which is in any case characteristic of many objects orbiting our solar system. If precession occurs in the plane of the orbit, its effect is to rotate the ellipse of the trajectory. The effect of this rotation will be slight for a low- e ellipse closely resembling a circle. The refresh time is the time it takes precession to change the orbit by D ; for an orbit with eccentricity e , this time is

$$t_{ref} = e^{-1} t_{ref,1}, \quad (27)$$

where $t_{ref,1}$ is the original estimate of the refresh time, $t_{prec} D/r$.

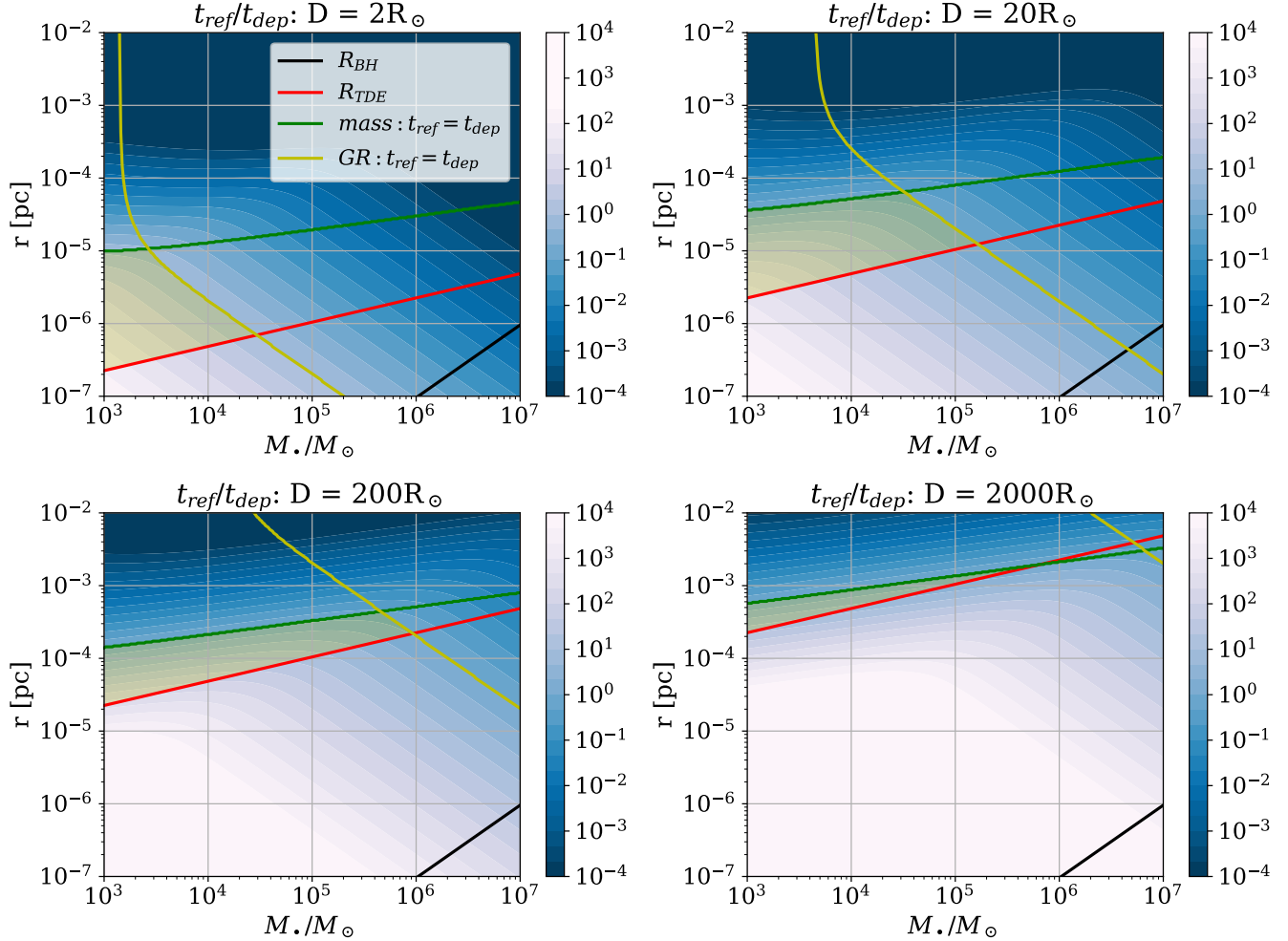


Figure 3. Color map of the ratio $t_{\text{ref}}/t_{\text{dep}}$ as a function of SMBH mass M_* and orbital radius r , for a star with mass M_\odot , and different collisional cross-sections (diameter from $2R_\odot$ to $2 \cdot 10^3 R_\odot$). The ratio is taken as the sum of reciprocals of equation 21 and equation 23. The black line is the Schwarzschild radius of the SMBH and the red line is the tidal disruption radius of a star with diameter D . The green line and the yellow line are the lines of equal t_{dep} and t_{ref} for mass and GR precessions (respectively). The light-yellow shaded region is where the ratio is greater than unity.

Another source of precession in asteroid belts is the perturbative gravitational pull of planets in the system. Let us assume most of this effect comes from the largest planet in the system, which we will call “Qupiter”. We denote Qupiter’s mass by m_Q and the semi-major axis of its trajectory a_Q . In the secular approximation, the precession time due to Qupiter is (Mustill & Wyatt 2009)

$$t_{\text{prec}}^Q = T \left(\frac{M_Q}{M_*} \right)^{-1} \cdot \max \left\{ \left(\frac{a_Q}{r} \right)^{-2}, \left(\frac{a_Q}{r} \right)^3 \right\}. \quad (28)$$

The ratio of depletion time to refresh time is then

$$\frac{t_{\text{dep}}}{t_{\text{ref}}^Q} = e \left(\frac{M_Q}{M_*} \right) \left(\frac{D}{r} \right)^{-2} \cdot \min \left\{ \left(\frac{a_Q}{r} \right)^2, \left(\frac{a_Q}{r} \right)^{-3} \right\}. \quad (29)$$

We can use equations 26 and 29 to determine D_c , the characteristic diameter above which we expect the collision rate to be less than the ergodic $n\Sigma v$ estimate. When secular precession from Qupiter dominates,

$$D_c^Q = 1.4 \cdot 10^8 \text{ km} \cdot e^{1/2} \left(\frac{M_Q}{M_*} \right)^{\frac{1}{2}} \cdot \min \left\{ \left(\frac{a_Q}{1 \text{ AU}} \right), \left(\frac{a_Q}{1 \text{ AU}} \right)^{-\frac{3}{2}} \left(\frac{r}{1 \text{ AU}} \right)^{\frac{5}{2}} \right\}. \quad (30)$$

While the effect of secular precession can always be dialed down by considering systems whose planets are lower in mass or more distant from the planetesimal belt, GR precession sets an unavoidable floor on D_c . In cases where the refresh time is set by GR precession,

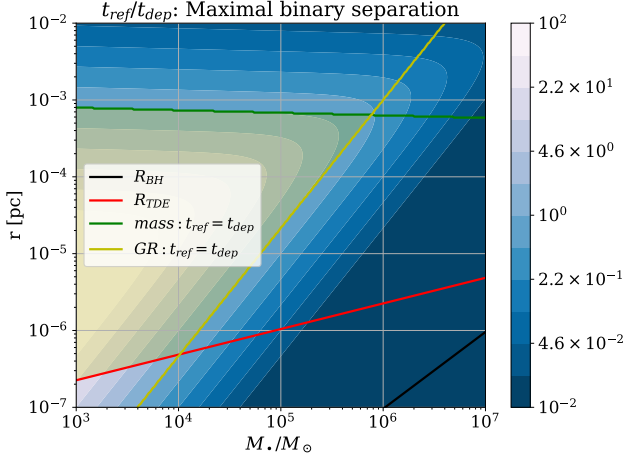


Figure 4. Color map of the ratio $t_{\text{ref}}/t_{\text{dep}}$ as a function of SMBH mass M_{\bullet} and radius r , for collisional ionization of a binary with maximal separation (as given by equation 25). The ratio is taken as the sum of reciprocals of equation 21 and equation 23. The black line is the Schwarzschild radius of the SMBH and the red line is the tidal disruption radius of a Sun-like star. The green line and the yellow line are the lines of equal t_{dep} and t_{ref} for mass and GR precessions (respectively). The light-yellow shaded region is where the ratio is greater than unity. Binary ionization rates can be 1-2 orders of magnitude lower than the $n\Sigma v$ limit inside the influence radius of intermediate mass black holes.

from equation 26, D_c will be

$$\begin{aligned} D_c^{\text{GR}} &= 2 \cdot 10^4 \text{ km} \cdot e^{1/2} \left(\frac{r}{1 \text{ AU}} \right)^{\frac{1}{2}} \left(\frac{M_{\star}}{M_{\odot}} \right)^{\frac{1}{2}} \\ &= 10^3 \text{ km} \cdot \left(\frac{e}{0.03} \right)^{\frac{1}{2}} \left(\frac{r}{1 \text{ AU}} \right)^{\frac{1}{2}} \left(\frac{M_{\star}}{0.1 M_{\odot}} \right)^{\frac{1}{2}}. \end{aligned} \quad (31)$$

It is clear from equation 31 that for planetesimal belts as distant as the Kuiper belt (i.e. located at $r > 30$ AU), around a star with mass $\gtrsim M_{\odot}$, the critical diameter will be greater than Earth’s diameter. That is true even taking into account the low eccentricity of the Kuiper belt’s “cold” population, for which $e \sim 0.03$ is representative (Petit et al. 2011). Asteroid belts with a smaller orbital radius, such as the asteroid belt in our own Solar system at ~ 2 AU, will generally have a smaller D_c . Even here, however, it is hard to get below $D_c \sim 10^{2-3}$ km unless one invokes a very dynamically cold planetesimal population.

Figure 5 shows D_c as a function of a perturbing planet’s (Qupiter’s) mass and semimajor axis, for a planetesimal belt at 1 AU with $e = 0.03$, and a central red dwarf with $M_{\star} = 0.1 M_{\odot}$. It can be seen that if Qupiter’s mass is less than about $10^{-3} M_{\star} = 0.1 M_{\text{Jupiter}}$ and its orbital radius is $\gtrsim 10$ AU, objects as large as the Earth

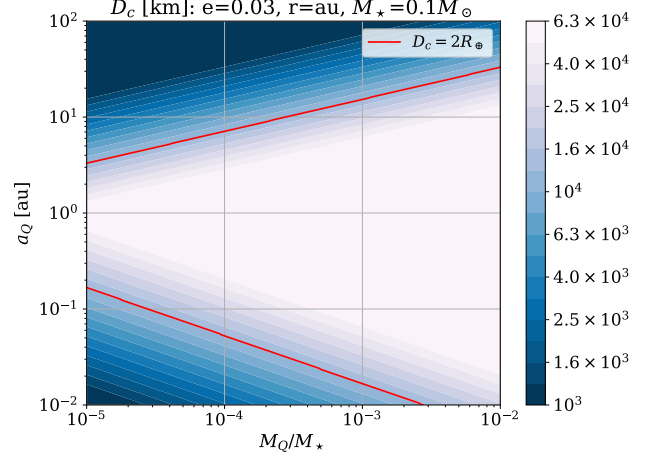


Figure 5. Color map of D_c as a function of the perturbing planet’s (Qupiter’s) mass and semimajor axis. D_c is calculated according to equations 30 and 31. The orbital eccentricity of planetesimals is taken to be 0.03, their orbital radius 1 AU, and the central star’s mass $M_{\star} = 0.1 M_{\odot}$. The red line indicates where D_c equals Earth’s diameter.

can experience a reduced collision rate. Deviations from ergodicity can extend to dwarf planet (e.g. Ceres) sizes only if no gas/ice giants are present, and furthermore the planetesimal belt is very low- e (with $e \ll 10^{-2}$).

4.3.2. Debris disks around white dwarves

The tidal disruption of asteroids and dwarf planets can produce very compact debris disks around white dwarf stars (Jura 2003; Metzger et al. 2012). The aftermath of such a planetesimal disruptions is observed as an infrared excess from the resulting dusty debris (Zuckerman & Becklin 1987; Debes et al. 2011), and current work estimates that a few percent of all white dwarves have this type of debris disk at any point in time (Farihi et al. 2009; Bonsor et al. 2017).

The main sources of precession for debris orbiting a white dwarf are GR, the bulk gravitation of the debris disk itself, and the quadrupole moment of the white dwarf (from e.g. rotational oblateness). Let us take the white dwarf and the debris disk from Manser et al. (2019) as an example, with the debris disk orbiting at $r \sim 5 \cdot 10^{-3}$ AU, and $M_{\star} = 0.7 M_{\odot}$. Using equation 31 for the critical diameter due to GR precession, and assuming $e \approx 0.01$, we get $D_c^{\text{GR}} \approx 100$ km.

Mass precession due to the debris disk’s gravitation gives $t_{\text{ref}} \sim \frac{D}{r} \frac{M_{\star}}{M_{\text{disk}}} T$. The critical radius due to mass precession is then

$$D_c^{\text{mass}} = \sqrt{e \frac{M_{\text{disk}}}{M_{\star}}} r. \quad (32)$$

For D_c^{mass} to be less than D_c^{GR} ,

$$M_{\text{disk}} < 3M_{\odot} \left(\frac{M_{\star}}{M_{\odot}} \right)^2 \left(\frac{r}{1\text{km}} \right)^{-1}. \quad (33)$$

In our case, this amounts to $M_{\text{disk}} < 2 \cdot 10^{-6} M_{\odot} = 0.6 M_{\oplus}$. That is, the critical radius will still be ~ 100 km if the total mass of the debris disk is less than about Earth’s mass.

Lastly, precession due to the white dwarf’s quadrupole moment J_2 is (Will 1993)

$$t_{\text{prec}} \sim J_2^{-1} T \left(\frac{r}{R_{\star}} \right)^2. \quad (34)$$

The quadrupole moment can be estimated $J_2 \sim \left(\frac{\omega}{\omega_c} \right)^2$, with the critical rotation frequency $\omega_c = \sqrt{GM_{\star}/R_{\star}^3}$. Equating $t_{\text{ref}} = e^{-1} \frac{D}{r} t_{\text{prec}}$ and $t_{\text{dep}} = \frac{r}{D} T$, we get the critical size

$$D_c^{\text{quad}} = \sqrt{e} R_{\star} \frac{\omega}{\omega_c}. \quad (35)$$

In our case, $R_{\star} = 7000$ km and $M_{\star} = 0.7 M_{\odot}$, so $\omega_c = 7 \cdot 10^3 \frac{2\pi}{\text{day}}$. To have $D_c^{\text{quad}} < 100$ km, the white dwarf must rotate slower than 10^3 times per day. As can be seen in Hermes et al. (2017), a more likely rotation period for a white dwarf is of the order of a few rotations per day; therefore, the WD quadrupole moment is likely a negligible contribution to precession.

To conclude, in debris disks with less mass than $\sim M_{\oplus}$ around slowly rotating white dwarves, it is possible for planetesimals with a diameter greater than $\sim 10^2$ km to experience a reduced, non-ergodic collision rate.

5. CONCLUSION

We have studied the collision rate in systems governed by degenerate potentials such as the Keplerian one and the harmonic oscillator. Although these perfect potentials represent idealizations of any astrophysical system, they are often quite good approximations of the densest star systems in the Universe, where interesting phenomena can arise from collisions or other close encounters between stars. Likewise, the Kepler potential is an excellent approximation for planetary and exoplanetary dynamics, where close encounter rates are of interest for e.g. understanding outcomes of collisional cascades.

We have shown that for individual realizations of such degenerate systems, the kinetic collision rate $n\Sigma v$ is not always valid. If collisions are non-destructive, an ensemble average over all possible realizations of a system will recover the $n\Sigma v$ rate, but specific realizations may differ greatly from it. In a spherical potential, $n\Sigma v$ will be essentially correct for most specific realizations. For the closed orbits of the Kepler potential and the harmonic

potential, most realizations will not have any collisions at all, while a few realizations will have a collision rate far higher than $n\Sigma v$.

In more realistic systems, collisions are destructive and orbits will never be perfectly closed, due to the effects of precession (i.e. bulk deviation from an idealized degenerate potential) and relaxation (i.e. deviations from the idealized degenerate potential sourced by small-scale, stochastic granularity). We have shown how to take these effects into account, and have categorized types of systems according to the formula required to calculate the collision rate; in an increasingly degenerate order, the categorization is: ergodic, Keplerian, semi-harmonic, and harmonic (see figure 2). The more degenerate a system is, the lower the rate of destructive collisions will be compared to $n\Sigma v$.

While these results suggest a potential failure of the usual $n\Sigma v$ formalism in the astrophysical contexts where collisions are of greatest interest, we have found that different physical effects will “save” the ergodic $n\Sigma v$ rate in almost all collisional environments. In isothermal star clusters (globulars and NSCs) lacking a massive central black hole, relaxation from two-body scatterings is the key physical effect that refreshes opportunities for pairwise collisions and recovers the $n\Sigma v$ rate; we find that deviations from ergodicity in these dense star clusters are wholly negligible. In the deeper potential wells of massive black holes, relaxation can be less efficient, and orbital intersections are generally refreshed by coherent precession (either from GR or from the extended mass of the star cluster around the black hole). While minor deviations from the $n\Sigma v$ collision rate can exist for some star-star collisions (figure 3, the most dramatic failure of ergodicity arises for binary ionizations inside the influence radius of intermediate mass black holes (figure 4)).

In debris disks and planetesimal belts, collisional cascades can in principle occur at rates below the typical $n\Sigma v$ one, although precession from GR as well as secular torques (from any large exoplanets in the star system) will restore the $n\Sigma v$ limit for most objects below the size of a dwarf planet. The impact of precession will be muted, however, for very dynamically cold planetesimal/debris disks.

At a high level of abstraction, there is no *a priori* reason why the $n\Sigma v$ formula should apply in nearly Keplerian or nearly harmonic potentials. The $n\Sigma v$ approach to collision rates assumes a uniform sea of targets, but in reality, configurations of particles orbiting in nearly degenerate potentials will usually, at any moment in time, lack *any* opportunities for particle-particle collision. We have shown that in different astrophysical examples of

nearly degenerate potentials, collisional dynamics recovers the $n\Sigma v$ limit due to varied combinations of GR precession, secular precession, and two-body relaxation. There is no universal pattern as to which effect dominates, and different astrophysical systems must be evaluated on a case-by-case basis to determine why orbits fail to close sufficiently. However, in all the examples we have considered, nearly degenerate potentials are almost never degenerate enough to avoid the classic $n\Sigma v$ collision rate formula, and so we conclude that $n\Sigma v$ is an *unreasonably effective* description of encounters in astrophysical environments.

DATA AVAILABILITY

The data that support the findings of this study are available within the article. The python scripts that created the figures in this article are available at <https://github.com/elishamod/Non-ergodic-collision-rates>.

- 1 This research was partially supported by an ISF, MOS
- 2 and an NSF/BSF grants. NCS gratefully acknowledges
- 3 support from the Israel Science Foundation (Individual
- 4 Research Grant 2565/19) and the Binational Science
- 5 Foundation (grant Nos. 2019772 and 2020397).

APPENDIX

A. EQUIVALENCE TO $n\Sigma v$ IN AN ENSEMBLE AVERAGE

A system with closed orbits and non-destructive collisions, may sometimes have a much greater collision rate than the ergodic rate $n\Sigma v$, and sometimes have no collisions at all. In this appendix we show that in an ensemble average, which is an average over all possible realizations of a distribution, the rate of collisions is precisely equal to the ergodic calculation. This result can be understood intuitively since in an ensemble average, the probability of encountering a particle in a volume dV is $n dV$, which is similar to the ergodic hypothesis used in the $n\Sigma v$ calculation.

The idea of the proof is that any distribution can be written as a sum or an integral over δ -functions, each representing a discrete particle. If we prove equivalence for a collision of two particles, represented by two orbits with δ -functions, then equivalence will be proven for a general distribution. Then, let us consider the problem of two particles, each in its own orbit. The $n\Sigma v$ calculation of total collision rate is

$$\text{rate} = \int dV n_1 n_2 \Sigma v. \quad (\text{A1})$$

The integrand only contributes at the intersection region, so we can assume that the trajectories of the two particles are the straight lines continued from the intersection. Let us choose our coordinate system such that particle 1 moves along the x axis, and particle 2's velocity is in the $x - y$ plane, at an angle α from \hat{x} . Let us define the origin as the location of particle 1 in the point of closest approach to particle 2's trajectory. Then, the particles' distributions can be written

$$\begin{aligned} n_1 &= \frac{\delta(y)\delta(z)}{v_1 T_1}, \\ n_2 &= \frac{\delta(x \sin \alpha - y \cos \alpha)\delta(z - \Delta)}{v_2 T_2}. \end{aligned} \quad (\text{A2})$$

where Δ is the distance between the trajectories at the closest point, v_i are the particles' velocities and T_i their periods. As it is, equation A1 will give zero collision rate for $\Delta \neq 0$. This is because when the distributions change on a scale smaller than $\sqrt{\Sigma}$, $n\Sigma v$ should actually be written as an integral of particle flux through the cross-section.

$$\text{rate} = \int dV n_1(\vec{r}) \int d\vec{A} \cdot (\vec{v}_2 - \vec{v}_1) n_2(\vec{r} + \vec{a}), \quad (\text{A3})$$

where \vec{r} is a volume integration variable and \vec{a} is an area integration variable. The inner integral is the flux of particle 2 on particle 1's cross-section, so it only covers the area of particle 1's cross-section. Let us do the inner integral with the parametrization $\vec{a} = \hat{e}R \cos \phi + \hat{z}R \sin \phi$, where \hat{e} is a unit vector perpendicular to both \hat{z} and $\vec{w} = \vec{v}_2 - \vec{v}_1$.

$$\begin{aligned} w \int_0^{2\pi} d\phi \int_0^d R dR n_2(\vec{r} + \hat{e}R \cos \phi + \hat{z}R \sin \phi) \\ = \frac{w}{v_2 T_2} \int_0^{2\pi} d\phi \int_0^d R dR \delta(z + R \sin \phi - \Delta) \cdot \delta[(x + R e_x \sin \phi) \sin \alpha - (y + R e_y \cos \phi) \cos \alpha] \end{aligned} \quad (\text{A4})$$

The inner integral is nonzero only if $0 \leq \frac{\Delta-z}{\sin \phi} \leq d$. Continuing,

$$= \frac{w}{v_2 T_2} \int_0^{2\pi} d\phi \frac{|\Delta-z|}{\sin^2 \phi} \delta \left[(x + e_x(\Delta-z)) \sin \alpha - (y + e_y(\Delta-z) \cot \phi) \cos \alpha \right]. \quad (\text{A5})$$

For the argument of this δ -function to vanish, $\cot \phi = \frac{(x+e_x(\Delta-z)) \tan \alpha - y}{e_y(\Delta-z)}$. This happens for two values of ϕ , offset by π . However, only one of them will have positive $\frac{\Delta-z}{\sin \phi}$, and we denote it by ϕ_0 . Carrying on

$$= \frac{w}{v_2 T_2} \frac{|\Delta-z|}{\sin^2 \phi_0} \cdot \frac{\sin^2 \phi_0}{|\Delta-z| e_y \cos \alpha} = \frac{w}{v_2 T_2 e_y \cos \alpha}. \quad (\text{A6})$$

It is important to remember that this is only true if $\frac{\Delta-z}{\sin \phi} \leq d$, otherwise it is zero. Taking the square of this inequality

$$\frac{(\Delta-z)^2}{\sin^2 \phi_0} = (\Delta-z)^2 (1 + \cot^2 \phi_0) = (z-\Delta)^2 + \left(\frac{(x+e_x(\Delta-z)) \tan \alpha - y}{e_y} \right)^2 \leq d^2. \quad (\text{A7})$$

Let us denote by $C(\vec{r})$ the function that is 1 if condition A7 is fulfilled, and 0 otherwise. We can do the full rate integral now:

$$\begin{aligned} \frac{w}{v_2 T_2 e_y \cos \alpha} \int d\vec{r} C(\vec{r}) n_1(\vec{r}) &= \frac{w}{v_1 T_1 v_2 T_2 e_y \cos \alpha} \int dx dy dz C(\vec{r}) \delta(y) \delta(z) \\ &= \frac{w}{v_1 T_1 v_2 T_2 e_y \cos \alpha} \int dx C(x, 0, 0). \end{aligned} \quad (\text{A8})$$

Plugging $y = z = 0$ into the condition in equation A7

$$\frac{(x - e_x \Delta)^2 \tan^2 \alpha}{e_y^2} \leq d^2 - \Delta^2 \quad \rightarrow \quad |x - e_x \Delta| \leq \sqrt{d^2 - \Delta^2} e_y \cot \alpha. \quad (\text{A9})$$

This means that $\int dx C(x, 0, 0) = 2\sqrt{d^2 - \Delta^2} e_y \cot \alpha$. Plugging this into the rate integral, we get

$$\text{rate} = \frac{2w\sqrt{d^2 - \Delta^2}}{v_1 T_1 v_2 T_2 \sin \alpha}, \quad (\text{A10})$$

which is precisely the same as equation 6, the result of the kinematic calculation in subsection 2.2. Therefore, we have proved that if collisions are non-destructive, the rate of collisions in an ensemble average is equal to the rate calculated under the assumption of ergodicity.

B. COMPARING MASS PRECESSION AND GRANULARITY IN SMBH ENVIRONMENTS

An orbital shuffling effect we have not taken into account in examining SMBH environments (subsection 4.2) is granularity – individual tugs from stars. As discussed in subsection 3.1, this is a random process so the refresh time it induces is

$$t_{\text{ref}}(\text{gran}) = \left(\frac{D}{R} \right)^2 t_{\text{relax}}, \quad (\text{B11})$$

as long as the effect of a single gravitational tug is less than D/R .

To estimate the relaxation time, we first consider an encounter with impact parameter b . Such an interaction makes a change Δv in a star's velocity

$$\Delta v \sim \frac{b G m}{v b^2} \sim v \frac{\bar{m}}{M_\bullet} \frac{r}{b}, \quad (\text{B12})$$

where \bar{m} is the mass of the encountered star, which we assume has the average stellar mass.

The rate of encounters with impact parameter $b \in [b, b+db]$ is given by the $n\Sigma v$ formula – $n \cdot 2\pi b db \cdot v = \frac{bv}{2r^2} \frac{dN}{dr} db$. Since this is a random walk process,

$$t_{\text{relax}}^{-1} = \frac{1}{v^2} \frac{d\langle v^2 \rangle}{dt} \sim \int n d\Sigma v \left(\frac{\Delta v}{v} \right)^2 \sim v \frac{dN}{dr} \left(\frac{\bar{m}}{M_\bullet} \right)^2 \int \frac{1}{b}. \quad (\text{B13})$$

We can estimate $\frac{dN}{dr} \sim \frac{1}{r} \frac{M(r)}{\bar{m}}$, where $M(r)$ is the accumulated stellar mass. Finally, we get

$$t_{\text{relax}} \sim \frac{1}{\log \frac{b_{\text{max}}}{b_{\text{min}}}} \frac{M_{\bullet}}{\bar{m}} \frac{M_{\bullet}}{M(r)} T. \quad (\text{B14})$$

The logarithm (Coulomb's logarithm) can be estimated as $\log \frac{b_{\text{max}}}{b_{\text{min}}} \sim \log \frac{r}{D}$, and will usually amount to about one order of magnitude. Considering that $M_{\bullet} \gg \bar{m}$, this means that $t_{\text{relax}} \gg t_{\text{prec}}$, where $t_{\text{prec}} = \frac{M_{\bullet}}{M(r)} T$.

To get the refresh times, the relaxation time is multiplied by $\left(\frac{D}{r}\right)^2$ while the precession time is multiplied by $\frac{D}{r}$. This would mean that the relaxation refresh time is shorter than the precession refresh time when

$$\frac{D}{r} < \log \left(\frac{r}{D} \right) \frac{\bar{m}}{M_{\bullet}}. \quad (\text{B15})$$

However, equation B15 is precisely the condition for the average stellar encounter to be enough for a refresh, making equation B11 invalid. The duration of the longest encounter is $\sim T$, meaning that for such a small D the refresh time is less than a period. Therefore, the cases where $t_{\text{ref}}(\text{relax}) < t_{\text{ref}}(\text{prec})$ will exhibit ergodic collision rates anyway. For this reason, there is no need to take granularity into account in subsection 4.2.

REFERENCES

- Antonini, F., & Rasio, F. A. 2016, *ApJ*, 831, 187, doi: [10.3847/0004-637X/831/2/187](https://doi.org/10.3847/0004-637X/831/2/187)
- Bahcall, J. N., & Wolf, R. A. 1976, *ApJ*, 209, 214, doi: [10.1086/154711](https://doi.org/10.1086/154711)
- Bailyn, C. D. 1995, *ARA&A*, 33, 133, doi: [10.1146/annurev.aa.33.090195.001025](https://doi.org/10.1146/annurev.aa.33.090195.001025)
- Balberg, S., Sari, R., & Loeb, A. 2013, *MNRAS*, 434, L26, doi: [10.1093/mnras/slt071](https://doi.org/10.1093/mnras/slt071)
- Balberg, S., & Yassur, G. 2023, *ApJ*, 952, 149, doi: [10.3847/1538-4357/acdd73](https://doi.org/10.3847/1538-4357/acdd73)
- Bertrand, J. 1873, *C. R. Acad. Sci.*, 77, 849–853
- Binney, J., & Tremaine, S. 2008, *Galactic Dynamics: Second Edition* (Princeton University Press)
- Bonsor, A., Farihi, J., Wyatt, M. C., & van Lieshout, R. 2017, *MNRAS*, 468, 154, doi: [10.1093/mnras/stx425](https://doi.org/10.1093/mnras/stx425)
- Brutman, Y., Steinberg, E., & Balberg, S. 2024, *ApJL*, 974, L22, doi: [10.3847/2041-8213/ad808f](https://doi.org/10.3847/2041-8213/ad808f)
- Chin, S. A. 2015, *American Journal of Physics*, 83, 320, doi: [10.1119/1.4901974](https://doi.org/10.1119/1.4901974)
- Clark, G. W. 1975, *ApJL*, 199, L143, doi: [10.1086/181869](https://doi.org/10.1086/181869)
- Dale, J. E., Davies, M. B., Church, R. P., & Freitag, M. 2009, *MNRAS*, 393, 1016, doi: [10.1111/j.1365-2966.2008.14254.x](https://doi.org/10.1111/j.1365-2966.2008.14254.x)
- Debes, J. H., Hoard, D. W., Wachter, S., Leisawitz, D. T., & Cohen, M. 2011, *ApJS*, 197, 38, doi: [10.1088/0067-0049/197/2/38](https://doi.org/10.1088/0067-0049/197/2/38)
- Dohnanyi, J. S. 1969, *J. Geophys. Res.*, 74, 2531, doi: [10.1029/JB074i010p02531](https://doi.org/10.1029/JB074i010p02531)
- Fabian, A. C., Pringle, J. E., & Rees, M. J. 1975, *MNRAS*, 172, 15, doi: [10.1093/mnras/172.1.15P](https://doi.org/10.1093/mnras/172.1.15P)
- Farihi, J., Jura, M., & Zuckerman, B. 2009, *ApJ*, 694, 805, doi: [10.1088/0004-637X/694/2/805](https://doi.org/10.1088/0004-637X/694/2/805)
- Fregeau, J. M., Chatterjee, S., & Rasio, F. A. 2006, *ApJ*, 640, 1086, doi: [10.1086/500111](https://doi.org/10.1086/500111)
- Generozov, A., Stone, N. C., Metzger, B. D., & Ostriker, J. P. 2018, *MNRAS*, 478, 4030, doi: [10.1093/mnras/sty1262](https://doi.org/10.1093/mnras/sty1262)
- Goodman, J., & Hut, P. 1989, *Nature*, 339, 40, doi: [10.1038/339040a0](https://doi.org/10.1038/339040a0)
- Grindlay, J. E., Heinke, C., Edmonds, P. D., & Murray, S. S. 2001, *Science*, 292, 2290, doi: [10.1126/science.1061135](https://doi.org/10.1126/science.1061135)
- Hailey, C. J., Mori, K., Bauer, F. E., et al. 2018, *Nature*, 556, 70, doi: [10.1038/nature25029](https://doi.org/10.1038/nature25029)
- Heggie, D. C. 1975, *MNRAS*, 173, 729, doi: [10.1093/mnras/173.3.729](https://doi.org/10.1093/mnras/173.3.729)
- Hermes, J. J., Kawaler, S. D., Romero, A. D., et al. 2017, *ApJL*, 841, L2, doi: [10.3847/2041-8213/aa6ffc](https://doi.org/10.3847/2041-8213/aa6ffc)
- Hills, J. G. 1976, *MNRAS*, 175, 1P, doi: [10.1093/mnras/175.1.1P](https://doi.org/10.1093/mnras/175.1.1P)
- Hills, J. G., & Day, C. A. 1976, *Astrophys. Lett.*, 17, 87
- Ivanova, N., Belczynski, K., Fregeau, J. M., & Rasio, F. A. 2005, *MNRAS*, 358, 572, doi: [10.1111/j.1365-2966.2005.08804.x](https://doi.org/10.1111/j.1365-2966.2005.08804.x)
- Ivanova, N., Heinke, C. O., Rasio, F. A., Belczynski, K., & Fregeau, J. M. 2008, *MNRAS*, 386, 553, doi: [10.1111/j.1365-2966.2008.13064.x](https://doi.org/10.1111/j.1365-2966.2008.13064.x)
- Ivanova, N., Heinke, C. O., Rasio, F. A., et al. 2006, *MNRAS*, 372, 1043, doi: [10.1111/j.1365-2966.2006.10876.x](https://doi.org/10.1111/j.1365-2966.2006.10876.x)
- Jura, M. 2003, *ApJL*, 584, L91, doi: [10.1086/374036](https://doi.org/10.1086/374036)

- Kremer, K., Ye, C. S., Rui, N. Z., et al. 2020, *ApJS*, 247, 48, doi: [10.3847/1538-4365/ab7919](https://doi.org/10.3847/1538-4365/ab7919)
- Levesque, E. M., Massey, P., Olsen, K. A. G., et al. 2005, *The Astrophysical Journal*, 628, 973, doi: [10.1086/430901](https://doi.org/10.1086/430901)
- Manser, C. J., Gänsicke, B. T., Eggl, S., et al. 2019, *Science*, 364, 66, doi: [10.1126/science.aat5330](https://doi.org/10.1126/science.aat5330)
- Merritt, D., Alexander, T., Mikkola, S., & Will, C. M. 2010, *PhRvD*, 81, 062002, doi: [10.1103/PhysRevD.81.062002](https://doi.org/10.1103/PhysRevD.81.062002)
- Metzger, B. D., Rafikov, R. R., & Bochkarev, K. V. 2012, *MNRAS*, 423, 505, doi: [10.1111/j.1365-2966.2012.20895.x](https://doi.org/10.1111/j.1365-2966.2012.20895.x)
- Mustill, A. J., & Wyatt, M. C. 2009, *Monthly Notices of the Royal Astronomical Society*, 399, 1403, doi: [10.1111/j.1365-2966.2009.15360.x](https://doi.org/10.1111/j.1365-2966.2009.15360.x)
- Neumayer, N., Seth, A., & Böker, T. 2020, *The Astronomy and Astrophysics Review*, 28, doi: [10.1007/s00159-020-00125-0](https://doi.org/10.1007/s00159-020-00125-0)
- Pan, M., & Sari, R. 2005, *Icarus*, 173, 342, doi: [10.1016/j.icarus.2004.09.004](https://doi.org/10.1016/j.icarus.2004.09.004)
- Petit, J.-M., et al. 2011, *Astron. J.*, 142, 131, doi: [10.1088/0004-6256/142/4/131](https://doi.org/10.1088/0004-6256/142/4/131)
- Pooley, D., Lewin, W. H. G., Anderson, S. F., et al. 2003, *ApJL*, 591, L131, doi: [10.1086/377074](https://doi.org/10.1086/377074)
- Portegies Zwart, S. F., & McMillan, S. L. W. 2000, *ApJL*, 528, L17, doi: [10.1086/312422](https://doi.org/10.1086/312422)
- Press, W. H., & Teukolsky, S. A. 1977, *ApJ*, 213, 183, doi: [10.1086/155143](https://doi.org/10.1086/155143)
- Reinoso, B., Leigh, N. W. C., Barrera-Retamal, C. M., et al. 2022, *MNRAS*, 509, 3724, doi: [10.1093/mnras/stab3254](https://doi.org/10.1093/mnras/stab3254)
- Rodriguez, C. L., Chatterjee, S., & Rasio, F. A. 2016, *PhRvD*, 93, 084029, doi: [10.1103/PhysRevD.93.084029](https://doi.org/10.1103/PhysRevD.93.084029)
- Schlichting, H. E., Fuentes, C. I., & Trilling, D. E. 2013, *AJ*, 146, 36, doi: [10.1088/0004-6256/146/2/36](https://doi.org/10.1088/0004-6256/146/2/36)
- Spitzer, Lyman, J., & Hart, M. H. 1971, *ApJ*, 166, 483, doi: [10.1086/150977](https://doi.org/10.1086/150977)
- Stone, N. C., & Metzger, B. D. 2016, *MNRAS*, 455, 859, doi: [10.1093/mnras/stv2281](https://doi.org/10.1093/mnras/stv2281)
- Tanaka, H., Inaba, S., & Nakazawa, K. 1996, *Icarus*, 123, 450, doi: [10.1006/icar.1996.0170](https://doi.org/10.1006/icar.1996.0170)
- Will, C. M. 1993, *The Classical Tests* (Cambridge University Press), 166–183, doi: [10.1017/CBO9780511564246.009](https://doi.org/10.1017/CBO9780511564246.009)
- Zuckerman, B., & Becklin, E. E. 1987, *Nature*, 330, 138, doi: [10.1038/330138a0](https://doi.org/10.1038/330138a0)